Electronic supplementary information

Single-layer Copper Particles Integrated with Carbon Nanotube Film for Flexible Electromagnetic Interference Shielding

Yuan Ma, Chao Lv, Zeng Tong, Chao Feng Zhao, Ye Sheng Li*, Ying Yan Hu, Yan Hong Yin, Xian Bin Liu, Zi Ping Wu*

School of Materials Science and Engineering, Jiangxi University of Science & Technology (JXUST), 86 Hongqi Road, Ganzhou 341000, P. R. China.

* Corresponding author. Tel: +86-797-8312422. Fax: +86-797-8312422.

E-mail: ysli@jxust.edu.cn (Y. S. Li), wuziping724@jxust.edu.cn (Z. P. Wu)

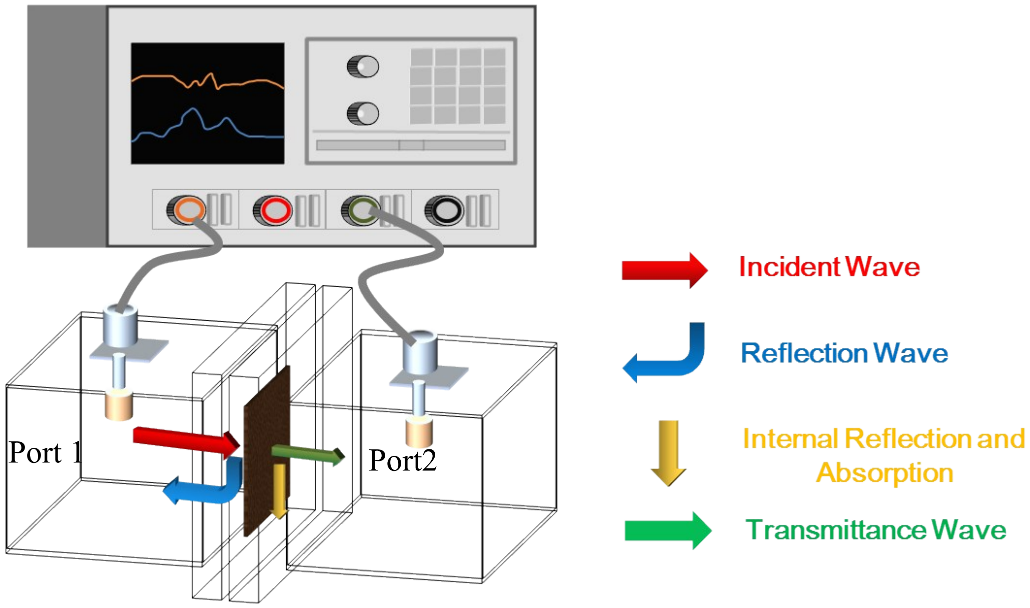

Fig. S1. The schematic diagram of the measurement of electromagnetic interference shielding setup

A rectangular waveguide via a two-port network analyzer system was used for measurement the EMI SE of the different samples. After the sample was cut into a rectangular sheet with an area slightly larger than the corresponding holder, it was held on the holder for S-parameter measurements (S_{11} and S_{21}).

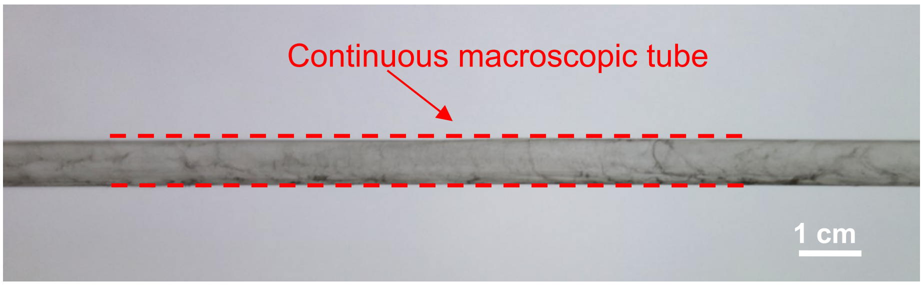

Fig. S2. The photograph of the continuous CNT macroscopic tube

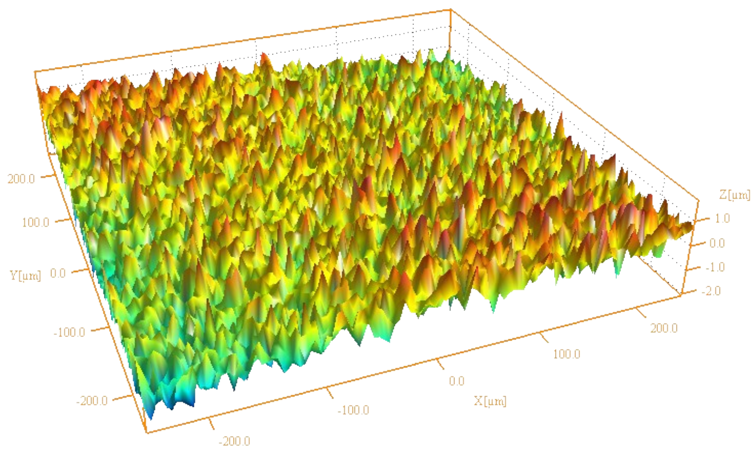

Fig. S3. The surface of the copper foil

Lot of microbumps with height of about ~1 µm on the surface of the copper foil that used as the substrate can be found obviously. These microbumps were embedded in the surface of the assembled macroscopic tube when it was been squeezed, thereby obtained CCTFs replicate the surface topography of the substrate.

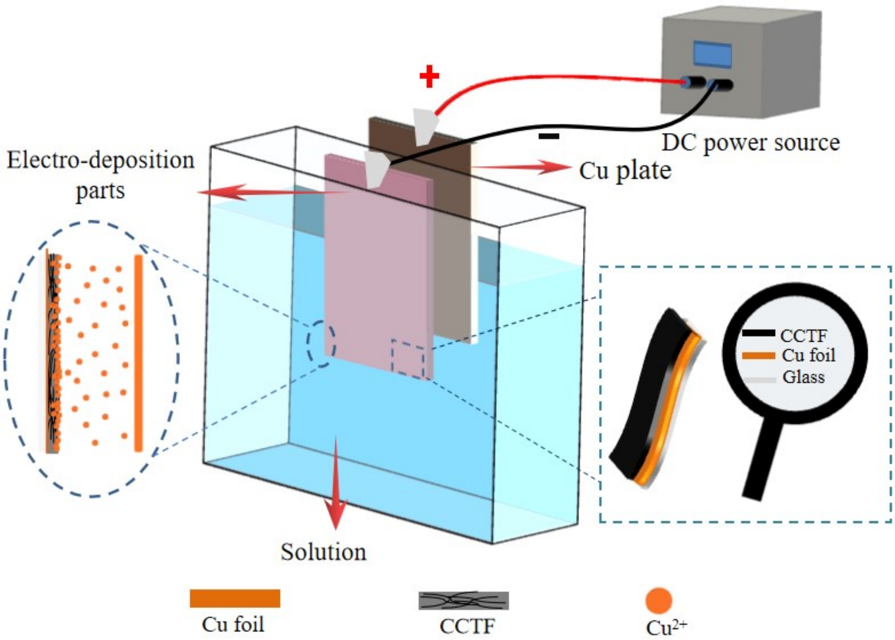

Fig. S4. The schematic diagram of electro-deposition setup

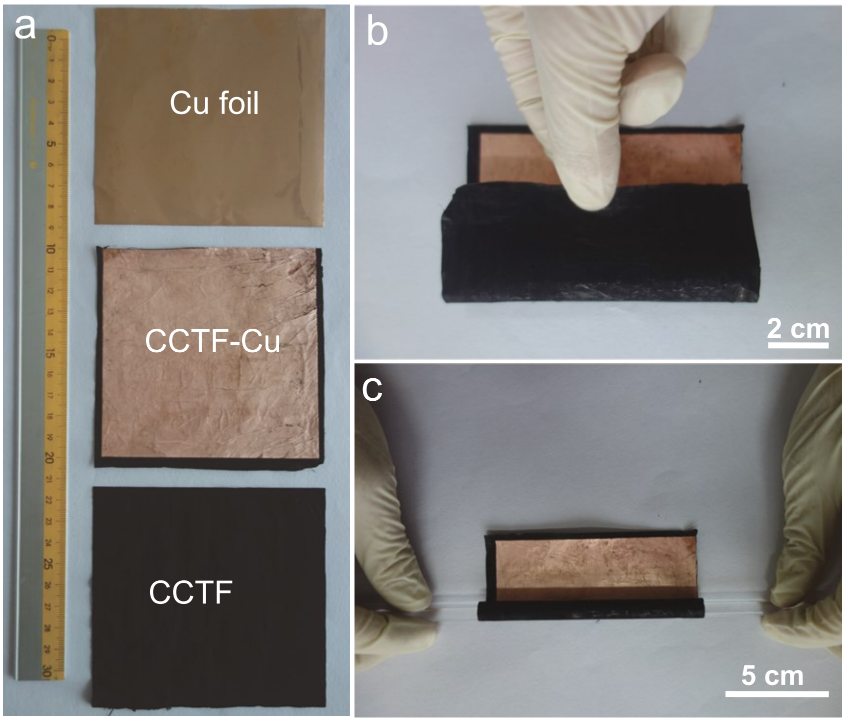

Fig. S5. The photographs of the CCTF-Cu and their flexibility, (a) the morphologies of Cu foil, CCTF-Cu and CCTF, qualitative demonstration of insensitivity of the composite towards (b) folding and (c) curling

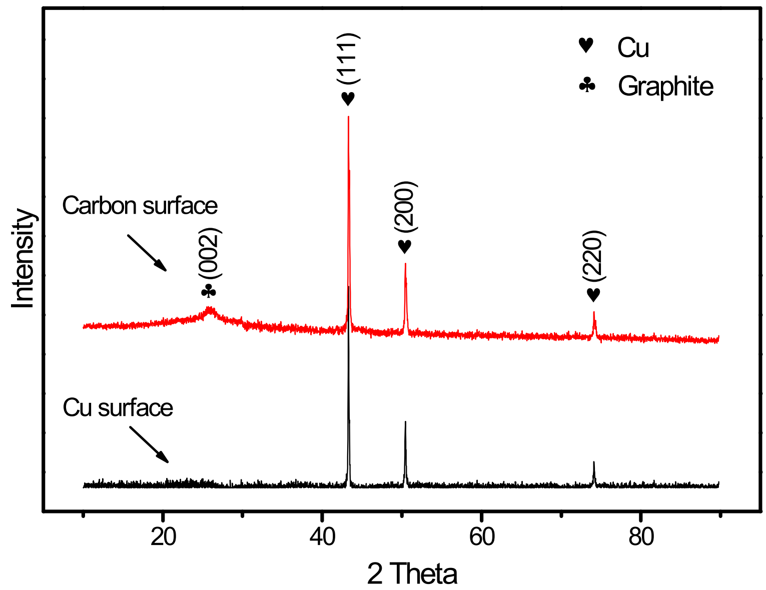

Fig. S6. The XRD patterns of CCTF-Cu composite film at different side

The different sides of the composite were checked by XRD. The diffraction characteristic peak for CCTF side located at 26.2° is corresponding to the (002) for graphite. In addition, the diffraction characteristic peaks 43.3°, 50.5° and 74.4° correspond to (111), (200), (101) and (220) plane for Cu, respectively. And copper also has been demonstrated by XRD pattern of the other side of the composite. The results indicated the copper particles have been successfully deposited onto the CCTF.

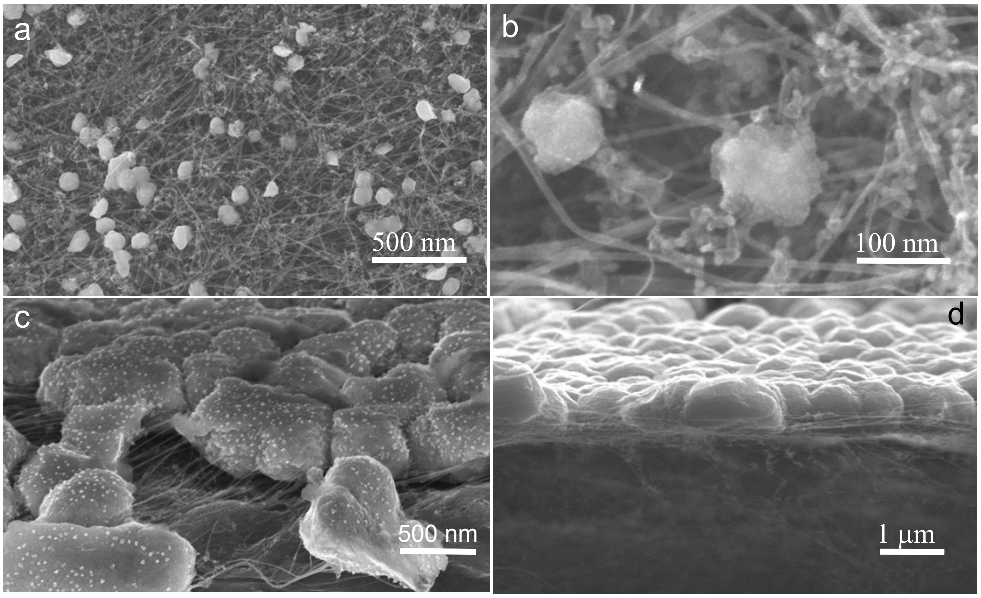

Fig. S7. The typical SEM images of the copper deposited on the CCTF's surface, (a) the low and (b) magnified images of copper particles inside the porous surface of the CCTF after deposition 10 seconds, the SEM image of the cross section of the copper deposited on the CCTF after (c) 60 and (d) 120 seconds

After electro-deposition 10 s, the particle on the surface of CCTF can be observed. And the magnified SEM images indicated the particles have infiltrated into the CCTF's surface. The porous surface provides enough positions for the sub-granular area of the obtained particles with diameter of ~ 100 nm, and thereby enhanced the contact area between the particles and CCTF. Moreover, the single-layer of particles with ~ 400 nm could be completely covered on the surface after deposition 60 s. It is interesting that the single-layer of particles on the surface also can be obtained even 120 s later. The difference is that the particles with long time deposition have integrated into bigger and flatter particles. The thickness of the composite film is ~ 2 μm can be seen clearly on the image.

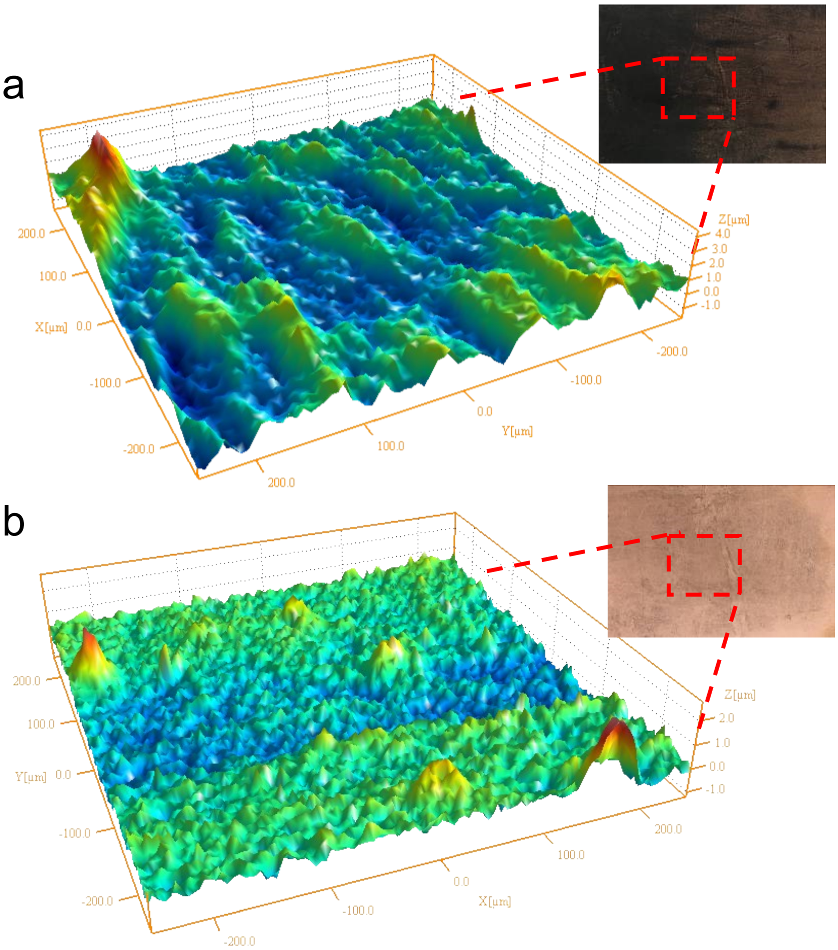

Fig. S8. The surface morphologies of the CNF assembled with (a) ethanol and (b) CCTF from compress macroscopic tube that deposited copper particles with 60 s

The morphologies of the samples that deposited copper with 60 s on CNFs and CCTFs show different colors. The CNF-Cu shows black on most of the areas, and small areas shows pale purple. The results demonstrate little copper particles have deposited. However, the CCTF-Cu shows uniform purple on the surface, which indicate copper particle deposited homogenous on the surface. In addition, the surface of the CCTF-Cu shows similar morphology to that of the CCTF.

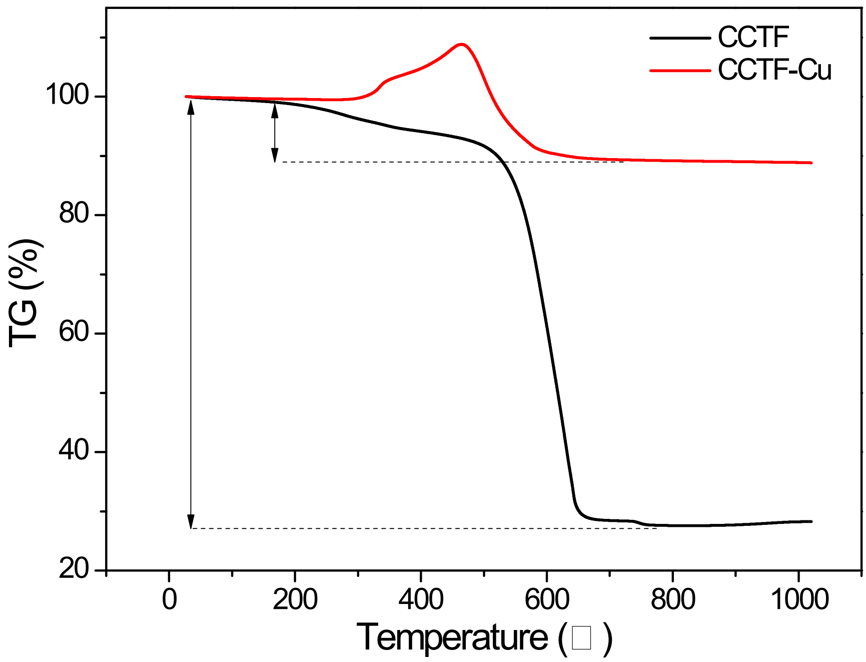

Fig. S9. The thermogravimetric curves of CCTF and CCTF-Cu (electro-deposition 60 s)

The content of Fe and Cu elements in the CCTF-Cu was tested by thermogravimetric analysis (Diamond TG/DTA6300) with the heating rate of 10 ^{o}C min^{-1} from room temperature to 1000 ^{o}C at an air flow rate of 100 ml min^{-1}. The weight loss below 400 ^{o}C could be attributed to the evaporation of H_2O and the oxidation of amorphous carbon. From 400 to 600 ^{o}C, there is a sharp weight loss in the samples, which is related to the consumption of graphitic walls of CNTs. And the oxidized process indicates the weight increase in the curve. After burning at high temperature, the weight of the residual material, which is presumably Fe_2O_3 and CuO. Therefore, the Cu content in the composite of ~ 80 wt% can be estimated.

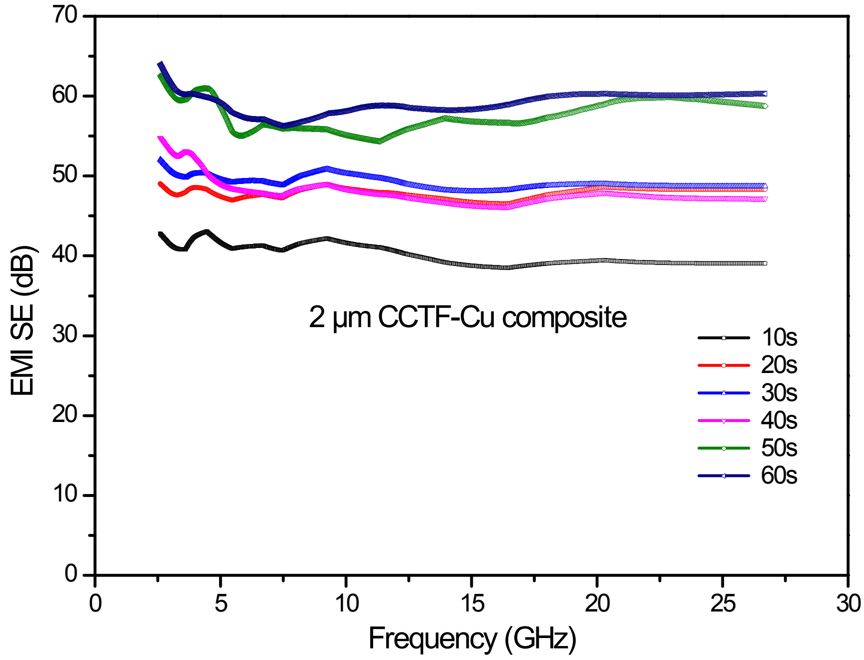

Fig. 10. The EMI SE performance of CCTF from electro-deposition copper particles within 60 s

The EMI SE increases obviously with the prolongation of the deposition until the time reaching 60 s. The SE is ~40 dB after the sample deposition Cu particles with 10 s, and the value suddenly increase to ~50 dB after the time prolong to 20 s. Moreover, the SE will increase to ~60 dB as the electro-deposition time extends to 60 s.

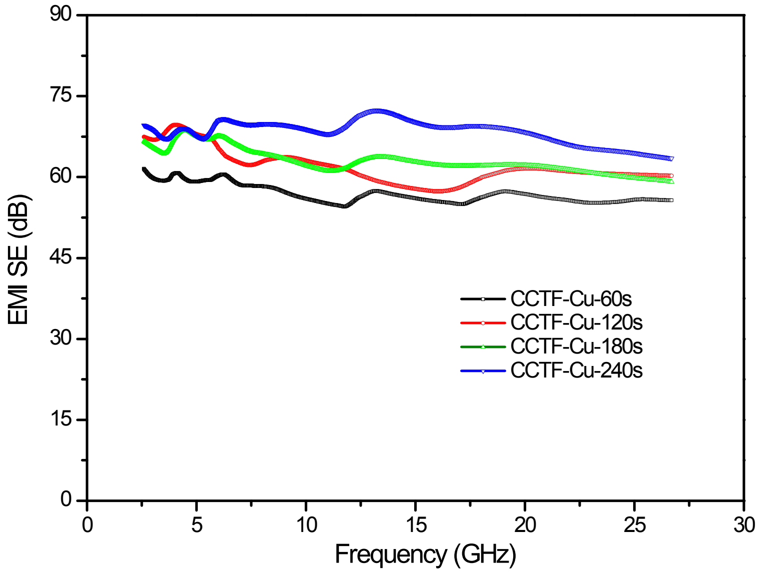

Fig. S11. Comparison of EMI SE performance of CCTF-Cu (a) under different electro-deposition time exceeds 60 s under a relative long electro-deposition time

After the electro-deposition time exceeds 60 s, the improvement of EMI SE performance of the CCTF-Cu composite increases slowly. The improved shielding performances are less than 10 dB as the electro-deposition time extended from 60 s to 240 s. The results indicate that it is difficult to achieving continuous SE improvement by prolonging the electro-deposition time and the thickness of the film.

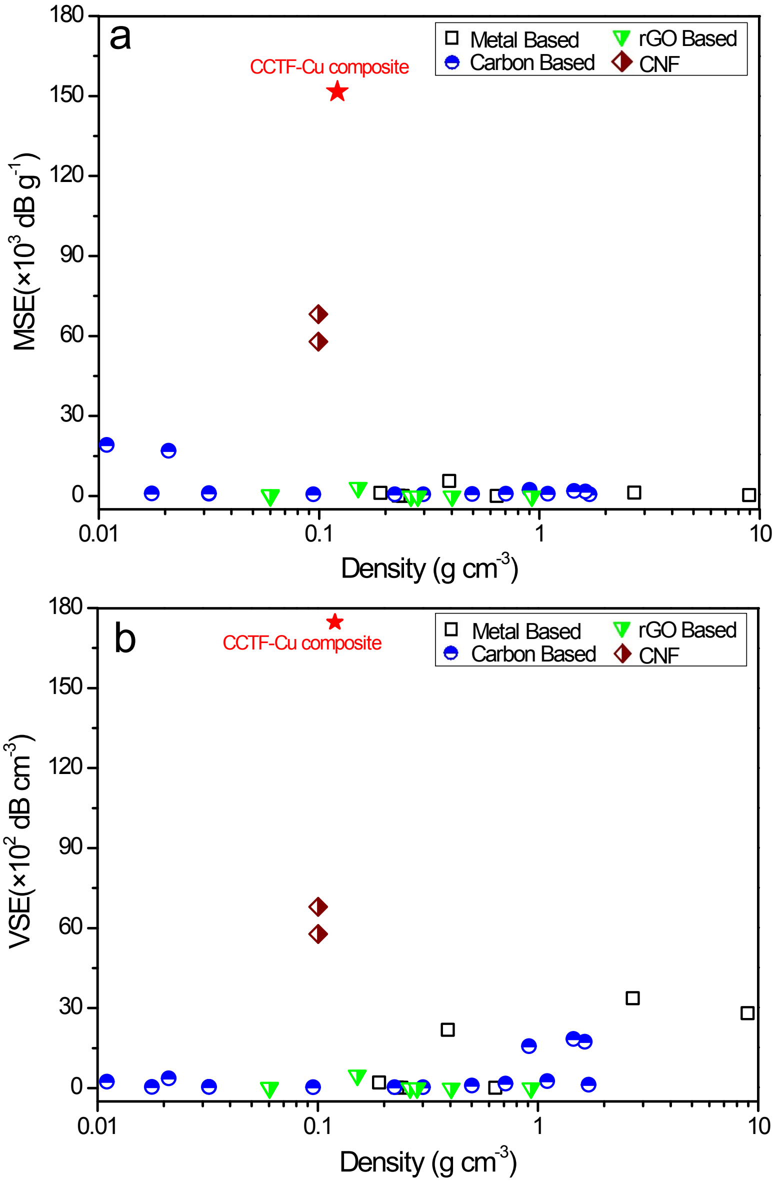

Fig. S12. Comparison of MSE (a) and VSE (b) for various flexible materials that have been reported in recent years

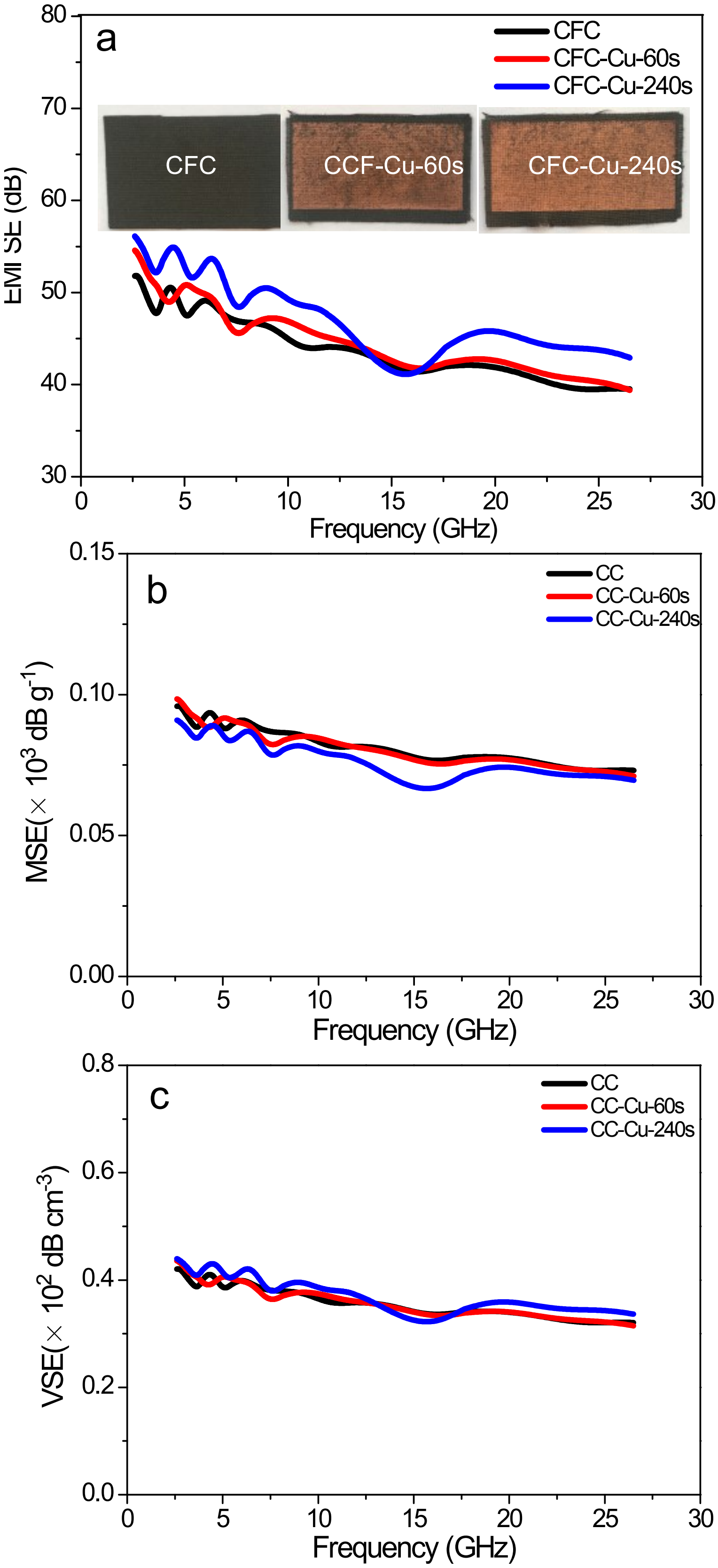

Fig. S13. The electromagnetic shielding performance (a), MSE (b) and VSE (c) of CFC and CFC-Cu, the insert images are the photographs of CFC and the obtained CFC-Cu with different deposited time. The area of the CFC as substrate is 5 cm× 8cm.

Table S1. The sheet electrical resistance of the CCTF-Cu composite after different electro-deposition time

Resistance	R1 Ω sq^{-1}	R2 Ω sq^{-1}	R3 Ω sq^{-1}	$R_{average}$
0 s	4.27	4.36	4.32	4.32
10 s	1.82	1.79	1.80	1.80
20 s	0.48	0.45	0.47	0.47
30 s	0.31	0.33	0.32	0.32
40 s	0.08	0.07	0.08	0.08
50 s	0.06	0.05	0.04	0.05
60 s	0.02	0.02	0.02	0.02

The sheet resistance the CCTF-Cu on Cu side was measured by a four-probe system, and the last column represents the average values of sheet electrical resistance of the different electro-deposition times. The results indicated CCTF-Cu has a significant improvement (from 4.32 Ω sq^{-1} increased to 0.02 Ω sq^{-1}) in electrical conductivity during the electro-deposition time.

Table S2. Comparison of EMI shielding performance for various flexible materials

Type	Materials	Frequency range (GHz)	Thickness mm	Density $g\ cm^{-3}$	EMI SE dB	MSE $dB\ g^{-1}$	VSE $dB\ cm^{-3}$	Ref.
Metal Based	Cu foil	8.2-12.4	0.01	8.97	70	318.2	2800	[1]
	Al foil	8.2-12.4	0.008	2.7	66	1245.2	3370.1	[1]
	Ni	8.2-12.4	1.95	N/A	23	N/A	N/A	[23]
	Ni-Co Fiber	8.2-12.4	2.5	N/A	41.2	N/A	N/A	[24]
	Ag/CF	8.2-12.4	2.5	N/A	38	N/A	N/A	[25]
	Ag Nanowires	8.2-12.4	0.8	N/A	33	N/A	N/A	[26]
	PP-SSF	8.2-12.4	3.1	0.64	48	9.8	6.3	[2]
	CuNi	8.2-12.4	1.5	0.24	25	28.4	6.8	[3]
	CuNi-CNT	8.2-12.4	1.5	0.23	54.6	65.0	14.9	[3]
	CuS/PANI	0.5-3	3	N/A	45.2	N/A	N/A	[37]
	$CoFe_2O_4$/PANI-PTSA	8.2-12.4	4	N/A	22.5	N/A	N/A	[34]
	$NiFe_2O_4$-$BaTiO_3$ ceramics	8.2-12.4	1.2	N/A	34	N/A	N/A	[36]
MXene Based	Ti_3C_2Tx-SA	8.2-12.4	0.045	N/A	90	N/A	N/A	[38]
	MXene foam	8.2-12.4	0.006	0.39	32	5614.0	2178.6	[4]
	Ti_3C_2Tx	8.2-12.4	0.045	N/A	92	N/A	N/A	[1]
	MXene/PS	8.2-12.4	2	N/A	62	N/A	N/A	[30]
	MXene/CNF	8.2-12.4	0.047	0.19	24	1097.9	208.6	[31]
	CF/PC/Ni film	0.03-1.5	0.31	1.7	72.7	56.4	95.8	[5]

MWCNT/WPU	8-12	2.3	0.032	46.7	259.4	8.3	[6]
GF-K2	2-18	0.031	1.63	130	1048.4	1713.1	[7]
MCMBs/MWCNTs/Fe_3O_4	8.2-12.4	0.5	0.5	80	130.7	65.4	[8]
Flexible graphite	0.03-1.5	0.2	1.1	110	203.7	224.7	[9]
MWCNT/PLA foam	8.2-12.4	2.5	0.3	23	12.8	3.8	[11]
PVDF/CNT	18-26.5	0.1	N/A	25	N/A	N/A	[27]
PVDF/CNT/graphene	18-26.5	0.1	N/A	27.6	N/A	N/A	[27]
CNT/CS foam	8.2-12.4	2.5	0.0176	37.6	349.1	8.47	[28]
CNT/cellulose	8.2-12.4	20	0.095	20.8	4.5	0.42	[29]
MWCNTs/Mn(nps)	8.2-12.4	0.13	0.711	42	185.6	131.9	[32]
CF/Fe_3O_4	1-18	13	N/A	20	N/A	N/A	[39]
CF/CNT	12.4-18	1	N/A	21.9	N/A	N/A	[40]
Graphene aerogel films	2-8	0.12	0.02	105	16422	328.5	[41]
CNT sponge	8.2-12.4	1	0.032	30	382.9	12.3	[42]
CNT/PDMS	8.2-12.4	2	N/A	46.3	N/A	N/A	[42]
CNT film	8.2-12.4	0.13	0.011	65	18568	204.2	[43]
CNT/PP	8.2-12.4	2	N/A	43.1	N/A	N/A	[44]
GF	2-18	0.013	0.91	48.9	1688.5	1536.5	[45]
GCF	2-18	0.015	1.45	57.6	1248.2	1809.9	[45]
C/SiO_2/SiC aerogels	12.4-18	10	0.223	24	4.4	0.98	[33]
rGO-PDMS	8-12	1	0.06	20	133.3	8.2	[10]
rGO-PS	8.2-12.4	2.5	0.26	45.1	28.4	7.4	[14]

	rGO-PEI	8.2-12.4	2.3	0.92	22	4.25	3.9	[15]
	rGO/Fe_3O_4-PEI	8-12	2.5	0.4	18	7.35	2.9	[16]
	Graphene foam	8.2-12.4	0.3	0.06	25	568.2	34	[17]
	Graphene film	8-12	0.05	0.15	60	3260.8	490.2	[18]
	rGO/γ-Fe_2O_3-PANI	8-12.4	2.5	N/A	51	N/A	N/A	[19]
	rGO/ MnO_2	12.4-18	3	N/A	57	N/A	N/A	[20]
	rGO-$BaTiO_3$	8.2-12.4	1.5	N/A	41.7	N/A	N/A	[21]
	rGO/CF/γ-Fe_2O_3	8.2-12.4	0.4	N/A	42.8	N/A	N/A	[22]
	rGO/CA film	8.2-12.4	0.012	N/A	25.7	N/A	N/A	[35]
	GNRs/MnO_2	12.4-18	3	N/A	57	N/A	N/A	[46]
	GNPs/rGO/EP	8.2-12.4	3	N/A	51	N/A	N/A	[47]
	PEI-rGO	8.2-12.4	4.5	N/A	26	N/A	N/A	[48]
	PI-rGO	8.2-12.4	0.8	0.28	21	38.3	10.7	[49]
CNT film Based	CNF	8.0-12.6	~0.004	0.1	67	68367.4	6842.3	[12]
	CNF	40-60	~0.004	0.1	57	58163.3	5821.1	[13]
	CCTF-Cu	2.6-26.5	~0.002	0.12	84	151724.1	17973.9	This work

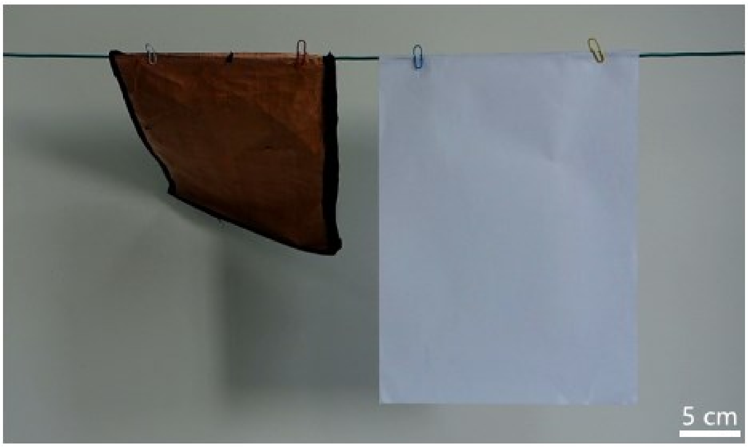

Movie S1. The light and flexible CCTF-Cu composite film.

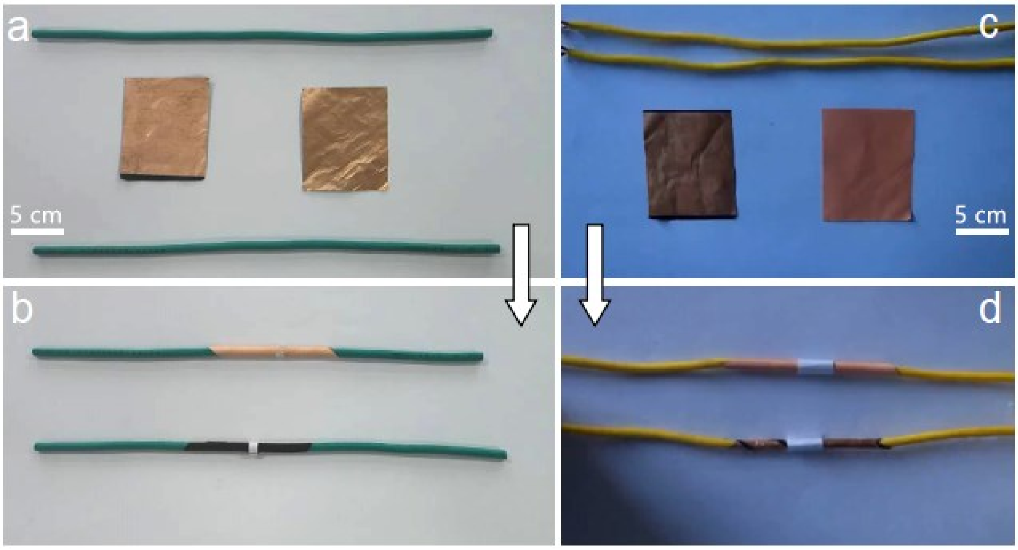

Movie S2. The demonstration of CCTF-Cu composite and commercial Cu foil wound on cables (CNT face (a, b) or Cu-face (c, d) toward outer side.

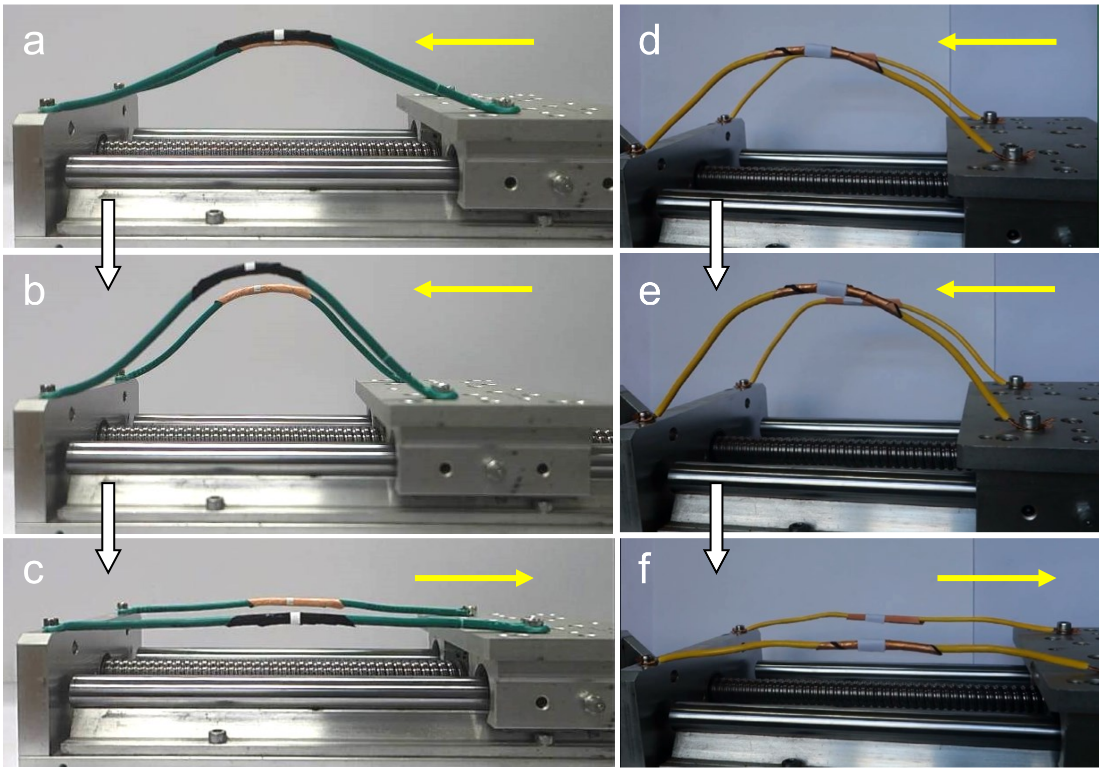

Movie S3. The demonstration of mechanical flexibility of CCTF-Cu composite (CNT face (a-c) and Cu-face (d-f) toward outer side)

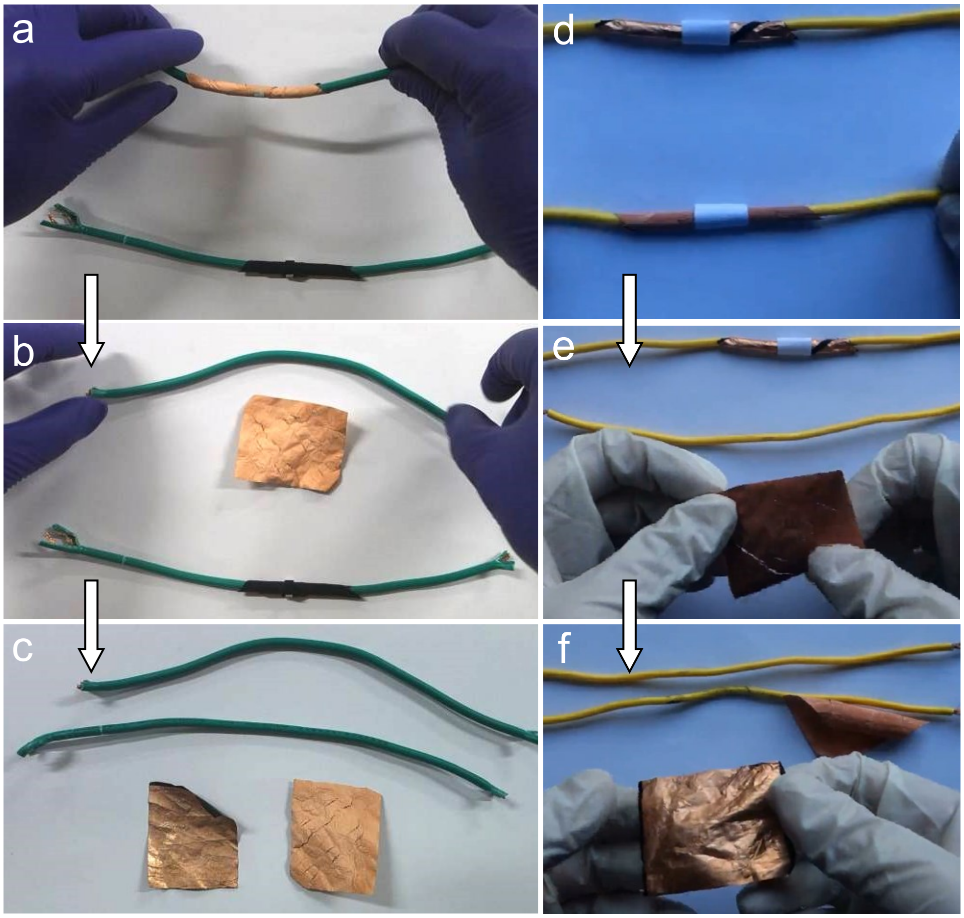

Movie S4. The demonstration of the morphologies of CCTF-Cu composite (CNT face (a-c) and Cu-face (d-f)) and commercial Cu foil after deformation

Movie S5. The demonstration of electromagnetic wave shielding with CCTF-Cu composite.

When the mobile phone was not been covered by the CCTF-Cu, the electromagnetic wave detector detected that the highest electromagnetic wave intensity is 17.80 μT. The screen of the mobile phone displays the calling successes, which indicates that the electromagnetic wave for communication has not been shielded. While the mobile phone was covered with the CCTF-Cu composite, the electromagnetic wave detector indicates that the electromagnetic wave has not been detected, and the electromagnetic wave intensity is 0 μT. This phenomenon suggests that the electromagnetic wave for communication was shielded successfully by the CCTF-Cu composite.

References

[1] Shahzad F., Alhabeb M., Hatter C. B., Anasori B., Hong S. M., Koo C. M., Gogotsi Y., Electromagnetic interference shielding with 2D transition metal carbides (MXenes), Science, 2016, 353, 1137-1140

[2] Ameli A., Nofar M., Wang S., Park C. B., Lightweight polypropylene/stainless-steel fiber composite foams with low percolation for efficient electromagnetic interference shielding, ACS Applied Materials & Interfaces, 2014, 6, 11091-11100

[3] Ji K., Zhao H., Zhang J., Chen J., Dai Z., Fabrication and electromagnetic interference shielding performance of open-cell foam of a Cu–Ni alloy integrated with CNTs, Applied Surface Science, 2014, 311, 351-356

[4] Liu J., Zhang H. B., Sun R., Liu Y., Liu Z., Zhou A., Yu Z. Z., Hydrophobic, flexible, and lightweight MXene foams for high-performance electromagnetic-interference shielding, Advanced Materials, 2017, 29, 1702367-1-6

[5] Xing D., Lu L., Teh K. S, Wan Z., Xie Y., Tang Y., Highly flexible and ultra-thin Ni-plated carbon-fabric/polycarbonate film for enhanced electromagnetic interference shielding, Carbon, 2018, 132, 32-41

[6] Zeng Z., Jin H., Chen M., Li W., Zhou L., Xue X., Zhang Z., Microstructure design of lightweight, flexible, and high electromagnetic shielding porous multi-walled carbon nanotube/polymer composites, Small, 2017, 13, 1701388-1-9

[7] Zhou E., Xi J., Liu Y., Xu Z., Guo Y., Peng L,, Gao C., Large-area potassium-doped highly conductive graphene films for electromagnetic interference shielding, Nanoscale, 2017, 9, 18613-18618

[8] Chaudhary A., Kumar R., Teotia S., Dhawan S. K., Dhakate S. R., Kumari S., Integration of MCMBs/MWCNTs with Fe_3O_4 in a flexible and light weight composite paper for promising EMI shielding applications, Journal of Materials Chemistry C, 2016, 5, 322-332

[9] Eddib A. A., Chung D. D. L., The importance of the electrical contact between specimen and testing fixture in evaluating the electromagnetic interference shielding effectiveness of carbon materials, Carbon, 2017, 117, 427-436

[10] Chen Z., Xu C., Ma C., Ren W., Cheng H. M., Lightweight and flexible graphene foam composites for high-performance electromagnetic interference shielding, Advanced Materials, 2013, 25, 1296-1300

[11] Kuang T., Chang L., Chen F., Sheng Y., Fu D., Peng X., Facile preparation of lightweight high-strength biodegradable polymer/multi-walled carbon nanotubes nanocomposite foams for electromagnetic interference shielding, Carbon, 2016, 105, 305-313

[12] Wu Z. P., Li M. M., Hu Y. Y., Li Y. S., Wang Z. X., Yin Y. H., Zhou X., Electromagnetic interference shielding of carbon nanotube macro-films, Scripta Materialia, 2011, 64, 809-812

[13] Wu Z. P., Cheng D. M., Ma W. J., Hu J. W., Yin Y. H., Hu Y. Y., Xu Q. F., Electromagnetic interference shielding effectiveness of composite carbon nanotube macro-film at a high frequency range of 40 GHz to 60 GHz, AIP Advances, 2015, 5, 388-394

[14] Zeng Z., Jin H., Chen M., Li W., Zhou L., Zhang Z., Lightweight and anisotropic porous MWCNT/WPU composites for ultrahigh performance electromagnetic interference shielding, Advanced Functional Materials, 2016, 26, 303-310

[15] Ling J., Zhai W., Feng W., Shen B., Zhang J., Zheng W. G., Facile preparation of lightweight microcellular polyetherimide/graphene composite foams for electromagnetic interference shielding. ACS Applied Materials & Interfaces, 2013, 5, 2677-2684

[16] Ling J., Zhai W., Feng W., Shen B., Zhang J., Zheng W. G., Facile preparation of lightweight microcellular polyetherimide/graphene composite foams for electromagnetic interference shielding. ACS Applied Materials & Interfaces, 2013, 5, 2677-2684

[17] Shen B., Li Y., Yi D., Zhai W., Wei X., Zheng W., Microcellular graphene foam for improved broadband electromagnetic interference shielding, Carbon, 2016, 102, 154-160

[18] Zhang L., Alvarez N. T., Zhang M., Haase M., Malik R., Mast D., Shanov V., Preparation and characterization of graphene paper for electromagnetic interference shielding, Carbon, 2015, 82, 353-359

[19] Singh A. P., Mishra M., Sambyal P., Gupta B. K., Singh B. P., Chandra A., Dhawan S. K., Encapsulation of γ-Fe_2O_3 decorated reduced graphene oxide in polyaniline core–shell tubes as an exceptional tracker for electromagnetic environmental pollution, Journal of Materials Chemistry A, 2014, 2, 3581-3593

[20] Yuan B., Bao C., Qian X., Song L., Tai Q., Liew K. M., Hu Y., Design of artificial nacre-like hybrid films as shielding to mitigate electromagnetic pollution, Carbon, 2014, 75, 178-189

[21] Gupta T. K., Singh B. P., Singh V. N., Teotia S., Singh A. P., Elizabeth I., Mathur R. B., MnO_2 decorated graphene nanoribbons with superior permittivity and excellent microwave shielding properties, Journal of Materials Chemistry A, 2014, 2, 4256-4263

[22] Singh A. P., Garg P., Alam F., Singh K., Mathur R. B., Tandon R. P., Dhawan S. K., Phenolic resin-based composite sheets filled with mixtures of reduced graphene oxide, γ-Fe_2O_3 and carbon fibers for excellent electromagnetic interference shielding in the X-band, Carbon, 2012, 50, 3868-3875

[23] Yu C. Q., Qin L. W., Fa L., Wan C. Z., Don G. Z., Graphene nanosheets/$BaTiO_3$ ceramics as highly efficient electromagnetic interference shielding materials in the X-band Journal of Materials Chemistry C, 2016, 4, 371-375

[24] Gargama H., Thakur A. K., haturvedi S. K., Polyvinylidene fluoride/nickel composite materials for charge storing electromagnetic interference absorption, and shielding applications, Journal of Applied Physics, 2015, 117, 224903-1-10

[25] Huang X., Dai B., Ren Y., Xu J., Zhu P., Preparation and study of electromagnetic interference shielding materials comprised of Ni-Co coated on web-like biocarbon nanofibers via electroless deposition, Journal of Nano-materials, 2015, 320306-1-7

[26] Li J., Qi S., Zhang M., Wang Z., Thermal conductivity and electromagnetic shielding effectiveness of composites based on Ag−plating carbon fiber and epoxy, Journal of Applied Polymer Science., 2015, 132, 42306-1-6

[27] Arjmand M., Moud A. A., Li Y., Sundararaj U., Outstanding electromagnetic interference shielding of silver nanowires: comparison with carbon nanotubes, RSC Advances, 2015, 5, 56590-56598

[28] Zhao B., Zhao C., Li R., Hamidinejad S. M., Park C. B., Flexible, ultrathin, and high-efficiency electromagnetic shielding properties of poly (vinylidene fluoride)/carbon composite films, ACS Applied Materials & Interfaces, 2017, 9, 20873-20884

[29] Li M. Z., Jia L. C., Zhang X. P., Yan D. X., Zhang Q. C., Li Z. M., Robust carbon nanotube foam for efficient electromagnetic interference shielding and microwave absorption. Journal of Colloid and Interface Science, 2018, 530, 113-119

[30] Huang H. D., Liu C. Y., Zhou D., Jiang X., Zhong G. J., Yan D. X., Li Z M., Cellulose composite aerogel for highly efficient electromagnetic interference shielding, Journal of Materials Chemistry A, 2015, 3, 4983-4991

[31] Sun R., Zhang H. B., Liu J., Xie X., Yang R., Li Y., Yu Z Z., Highly conductive transition metal carbide/carbonitride (MXene)@ polystyrene nano-composites fabricated by electrostatic assembly for highly efficient electromagnetic interference shielding, Advanced Functional Materials, 2017, 27, 1702807-1-11

[32] Cao W. T., Chen F. F., Zhu Y. J., Zhang Y. G., Jiang Y. Y., Ma M. G., Chen F., Binary strengthening and toughening of MXene/Cellulose nanofiber composite paper with nacre-inspired structure and superior electromagnetic interference shielding properties, ACS Nano, 2018, 12, 4583-4593

[33] Lu S., Bai Y., Wang J., Zhao C., Li W., Wang X., Huang Z., Researching on X-Band electromagnetic interference shielding efficiency of MWCNTs buckypapers inserted with Mn nanopowder, Nano, 2018, 13, 1850061-1-9

[34] Ismail M. M., Rafeeq S. N., Sulaiman J. M., Mandal A., Electromagnetic interference shielding and microwave absorption properties of cobalt ferrite $CoFe_2O_4$/polyaniline composite, Applied Physics A, 2018, 124, 380-391

[35] An Z., Ye C., Zhang R., Qu Q., Multifunctional C/SiO_2/SiC-based aerogels and composites for thermal insulators and electromagnetic interference shielding, Journal of Sol-Gel Science and Technology, 2019, 89, 1-11

[36] Jia L. C., Sun W. J., Zhou C. G., Yan D. X., Zhang Q. C., Li Z, M., Integrated strength and toughness in graphene/calcium alginate films for highly efficient electromagnetic interference shielding, Journal of Materials Chemistry C, 2018, 6, 9166-9174

[37] Qing Y., Ma L., Hu X., Luo F., Zhou W., $NiFe_2O_4$ nanoparticles filled $BaTiO_3$ ceramics for high-performance electromagnetic interference shielding applications, Ceramics International, 2018, 44, 8706-8709

[38] Sun J., Shen Y., Hu X. S., Polyaniline/flower-like CuS composites with improved electromagnetic interference shielding effectiveness, Polymer Bulletin, 2018, 75, 653-667

[39] Li Z., Wang Z., Lu W., Hou B., Theoretical study of electromagnetic interference shielding of 2D MXenes films, Metals, 2018, 8, 652-659

[40] Crespo M., Méndez N., González M., Baselga J., Pozuelo J., Synergistic effect of magnetite nanoparticles and carbon nanofibres in electromagnetic absorbing composites, Carbon, 2014, 74, 63-72

[41] Yang Y., Gupta M. C., Dudley K. L., Towards cost-efficient EMI shielding materials using carbon nanostructure-based nano composites, Nanotechnology, 2007, 18, 345701-1-5

[42] Xi J., Li Y., Zhou E., Liu Y., Gao W., Guo Y., Gao C., Graphene aerogel films with expansion enhancement effect of high-performance electromagnetic interference shielding, Carbon, 2018, 135, 44-51

[43] Lu D., Mo Z., Liang B., Yang L., He Z., Zhu H., Gui X., Flexible, lightweight carbon nanotube sponges and composites for high-performance electromagnetic interference shielding, Carbon, 2018, 133, 457-463

[44] Lu S., Shao J., Ma K., Chen D., Wang X., Zhang L., Ma J., Flexible, mechanically resilient carbon nanotube composite films for high-efficiency electromagnetic interference shielding, Carbon, 2018, 136, 387-394

[45] Wu H. Y., Zhang Y. P., Jia L. C., Yan D. X., Gao J. F., Li Z. M., Injection molded segregated carbon nanotube/polypropylene composite for efficient electromagnetic interference shielding, Industrial & Engineering Chemistry Research, 2018, 57, 12378-12385

[46] Li Y., Pei X., Shen B., Zhai W., Zhang L., Zheng W., Polyimide/graphene composite foam sheets with ultrahigh thermostability for electromagnetic interference shielding, RSC Advances, 2015, 5, 24342-24351

[47] Zhou E., Xi J., Guo Y., Liu Y., Xu Z., Peng L., Gao C., Synergistic effect of graphene and carbon nanotube for high-performance electromagnetic interference shielding films, Carbon, 2018, 133, 316-322

[48] Liang C., Qiu H., Han Y., Gu H., Song P., Wang L., Gu J., Superior electromagnetic interference shielding 3D graphene nanoplatelets/reduced graphene oxide foam/epoxy nanocomposites with high thermal conductivity, Journal of Materials Chemistry C, 2019, 7, 2725-2733

[49] Sawai P., Chattopadhaya P. P., Banerjee S., Synthesized reduce graphene oxide (rGO) filled polyetherimide based nanocomposites for EMI Shielding applications, Materials Today: Proceedings, 2018, 5, 9989-9999